Available online at www.sciencedirect.com
SCIENCE DIRECT®
Physica D 197 (2004) 174–195
PHYSICA D
www.elsevier.com/locate/physd

Rigid transition to the stationary structure and imposed convective instability in a reaction–diffusion system with flow

P.V. Kuptsov*

Department of Informatics, Saratov State Law Academy, Chernyshevskogo 104, Saratov 410056, Russia

Received 13 April 2003; received in revised form 25 March 2004; accepted 24 June 2004

Communicated by Dr. A. Doelman

Abstract

Stationary flow and diffusion distributed structure (FDS) is known to appear in a reaction–diffusion system with open flow when the constant perturbation is applied at the inlet. Usually, the FDS is considered in the oscillatory Hopf domain when the instability of the Hopf mode is convective. This paper focuses on the formation of the FDS in presence of the absolute Hopf instability. In this case, both FDS and Hopf solutions tend to invade the space. The result of this competition depends on the amplitude of the inflow perturbation and on the flow rate. At large flow rate the Hopf solution dominates if the inflow perturbation is small. Increasing of the inflow perturbation gives rise the rigid transition to FDS and produces the imposed convective Hopf instability. Small flow rate always gives an advantage to the Hopf solution. The FDS solution, though still appears near the inlet at large inflow perturbation, does not expand, and the FDS-Hopf domain boundary stays in a fixed position.

PACS: 82.40.Bj; 47.54.+r

Keywords: Rigid transition to FDS; Imposed convective instability; FDS-Hopf competition; Inflow perturbation; Reaction–diffusion system; Open flow; Pattern formation

1. Introduction

Reaction–diffusion systems typically demonstrate Hopf and Turing instabilities. The Hopf instability is associated with the appearance of the spatially homogeneous oscillations. The Turing instability emerges when the diffusion rates of reacting species are significantly different and results in the formation of a stationary spatially periodic structure.

* Present address: Centre for Mathematics, School of Engineering and Mathematical Sciences, City University London, Northampton Square, London EC1V 0HB, UK. Tel.: +7 8452 253346; fax: +7 8452 250453.

E-mail address: kupav@mail.ru (P.V. Kuptsov).

0167-2780/$ – see front matter © 2004 Elsevier B.V. All rights reserved.
doi:10.1016/j.physd.2004.06.013

In presence of an open flow, the instability is either absolute or convective [1–6]. If the flow rate is small, the diffusion carries the perturbation upstream faster than the flow sweeps it downflow. As a result, the perturbation invades the whole space. This situation is referred to as an absolute instability. If the flow rate is large, the flow acts faster than the diffusion do. Therefore, the perturbation asymptotically decays towards zero at every fixed point. This is the case of the convective instability. The transition between these two cases happens at the critical flow rate v_{ca} that can be determined from the set of equations [7–9] (see also references therein):

$$d(s,q)=0, \qquad \mathrm{Re}\, s(q)=0, \qquad \frac{\partial d/\partial q}{\partial d/\partial s}=0. \tag{1}$$

Here, $d(s,q)$ is the dispersion relation of the system under consideration, and s and q are, respectively, the complex frequency and the wave number of the elementary wave e^{st+qx}.

Another well known type of instability arises in the reaction–diffusion-flow systems when the reacting species have different flow rates [10]. This is referred to as a differential-flow instability (DIFI).

Recently, a new type of pattern formation mechanism was discovered that does not require the differential transport. The stationary periodic structure may arise in a reaction–diffusion-flow system in the oscillatory domain when the constant inhomogeneous perturbation is applied at the inlet. Provided that flow rate is sufficiently high, the flow distributes the temporal oscillations in space, and the phase of this spatial mode is frozen at the inflow boundary. This effect was reported by Kuznetsov et al. [9], and little bit later this was studied in more details by Andresén et al. [11]. Soon after these structures was observed experimentally by Kærn and Menzinger [12–14]. They referred to these as flow distributed oscillations (FDO). The combined action of flow and diffusion was studied by Satnoianu et al. [15,16]. The periodic patterns arising in this case are referred to as flow and diffusion distributed structures (FDS).

The FDS attracts much of interest. Kuptsov et al. [17] considered the perturbation of the FDS by the particle that is dragged by the flow and partially blocks it. For certain parameter values several peaks of the structure disappears, and the wave of substitution of the missing peaks runs across the structure. In other regimes the response with intermittent Hopf- and Turing-type structures is observed. In [18] by Kuptsov et al., the FDS was analyzed for the complex Ginzburg–Landau equation. In particular, the rigid transition to FDS was discussed. Satnoianu et al. [16] showed that the FDS mechanism is a robust morphogenetic mechanism which is more flexible in comparison with the classical Turing scenario. Kærn et al. [19,20] discussed the application of the concept of FDS for the modelling of the axial growth and segmentation in biology. Kærn and Menzinger in [21] reviewed a lot of experiments on FDS. Bamforth et al. [22] provided the experimental study of formation of the FDS. Taylor et al. [23] studied the competition between the FDS and the oscillating solution when the flow rate is close to the critical value.

The FDS solution exists when the flow rate v exceeds the critical value v_{st} [9]. If, in addition, the instability in the system is convective, i.e., $v > v_{ca}$, even very small inflow perturbation grows to the FDS [9,11]. It this case that is studied usually [21]. We refer to this as a soft transition to FDS. In this paper, we investigate the FDS in presence of the absolute Hopf instability, i.e., when $v_{st} < v < v_{ca}$. Selection of the FDS solution in this case occurs only if the inflow perturbation is sufficiently large, while the small inflow perturbation does not grow to the FDS and the Hopf oscillations appear instead. This case we refer to as a rigid transition to FDS. In paper [18], we reported the rigid transition to FDS for the complex Ginzburg-Landau equation. This paper analyzes the details of this transition for a reaction–diffusion system. As a concrete example, we consider the one-dimensional Brusselator model with flow.

We consider the FDS for the model system in the Hopf instability domain. (The conditions of arising of the FDS solution are analyzed in [9,11,15,16].) The flow rate is supposed to be the same for all species; thus, the effect of the differential flow is not taken into account. Most of discussions are done for the similar diffusion rates, but provided qualitative results are valid for the differential diffusion too.

Section 2 contains the brief review of instabilities in the Brusselator model. The plane of parameters is also obtained where the domains of soft as well as rigid transition to FDS are outlined. Section 3 presents the main phenomenology discussed in this paper. The series of the spatio-temporal diagrams illustrate the FDS-Hopf competition in the domain of rigid transition. In Section 4, the analysis is provided for the considered effects. Section 5 contains the discussion of possible manifestation of the rigid transition to FDS in experiments. Concluding Section 6

summarizes the obtained results, and in the Appendix more illustrations of the discussed effects are presented for two others reaction–diffusion system with flow.

2. Instabilities in the Brusselator model with flow

The Brusselator is one of the canonical models of reaction–diffusion systems under far-from-equilibrium conditions [24]. In presence of flow and diffusion, this is specified by the following set of equations [9]:

$$\frac{\partial U}{\partial t} + v\frac{\partial U}{\partial x} = A - (B+1)U + U^2V + \sigma\frac{\partial^2 U}{\partial x^2}, \qquad \frac{\partial V}{\partial t} + v\frac{\partial V}{\partial x} = BU - U^2V + \frac{\partial^2 V}{\partial x^2}. \tag{2}$$

Here, U and V denote the dynamical variables, $A > 0$ and $B > 0$ are the control parameters, $0 < \sigma$ is the ratio of the diffusion constants for U and V, and $v > 0$ is the flow rate. The flow is supposed to be directed from the left towards the right.

System (2) has a homogeneous steady state

$$U_S = A, \qquad V_S = \frac{B}{A}. \tag{3}$$

The linear stability of this state is described by the dispersion relation [9]

$$d(s,q) = (s + vq - B + 1 - \sigma q^2)(s + vq + A^2 - q^2) + A^2 B, \tag{4}$$

where s and q are, respectively, complex frequency and wave number of the elementary wave e^{st+qx}. Analysis of Eq. (4) gives the thresholds for the Hopf and Turing instabilities [25,9]:

$$B = B_H \equiv 1 + A^2 \quad \text{and} \quad B = B_T \equiv (1 + A\sqrt{\sigma})^2. \tag{5}$$

Below we consider the Hopf instability assuming that $B_H < B < B_T$.

The transition from absolute to convective instability occurs when the flow rate attains v_{ca}. This critical value can be obtained from the set of Eqs. (1) and (4) [9]. The FDS solution exists when $v > v_{st}$. The critical flow rate v_{st} can be found from the dispersion equation $d(s,q) = 0$ (4) as a bifurcation point for the spatial mode $s = 0$ [9]:

$$v_{st} = \sqrt{\frac{B^2 + (1 - A^2\sigma)^2 - B(2 + A^2(1+\sigma^2))}{(1+\sigma)(1 + A^2 - B)}}. \tag{6}$$

Fig. 1 shows the dependencies of v_{st} and v_{ca} on the parameter B. The curves in this figure divide the plane onto the four domains. The FDS solution exists above the curve $v_{st}(B)$ (domains I and II), while below this curve the inflow perturbation always decays in space (domains III and IV). The instability in the system (2) is absolute below the curve $v_{ca}(B)$ (domains II and III), and this is convective above the curve (domains I and IV). The critical flow rate v_{ca} is zero at $B = B_H$, and the steady state is stable for $B < B_H$.

In the domain I, the Hopf mode is convectively unstable and decays in every fixed point. Hence, it does not prevent the spatial growth of any inhomogeneous constant inflow perturbation to the FDS. This situation was reported by Kuznetsov et al. [9] and studied little bit later both theoretically by Andresén et al. [11] and experimentally by Kærn and Menzinger [12]. This is the case of the soft transition to the FDS.

In the domain II, the Hopf mode is absolutely unstable, i.e., both the FDS and the Hopf solutions tend to invade the whole space. A kind of competition of these solution should, obviously, be observed in this case. As shown below, this competition is controlled by the inflow perturbation and by the flow rate.

In the domain III, only the Hopf solution tends to spread over the space, because this is absolutely unstable and the FDS solution does not exist.

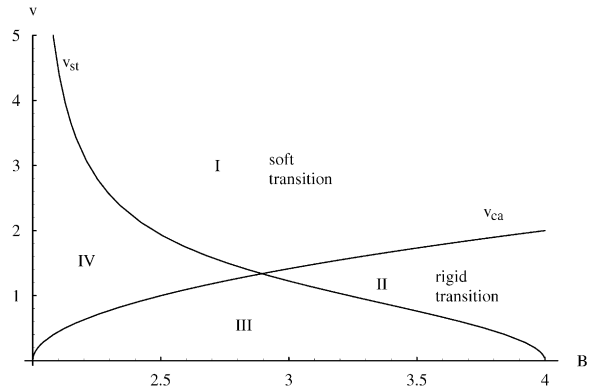

Fig. 1. Plane of parameters (B, v) for the system (2). v_{ca} is the critical flow rate for the transition from the convective instability (domains marked by the roman numbers I and IV) to the absolute instability (domains II and III), see Eqs. (1) and (4). v_{st} is the critical flow rate above which the FDS solution exists (domains I and II), see Eq. (6). The system becomes stable at $B = B_H = 2$. v_{ca} is zero in this point while v_{st} diverges. The plane is drawn for the parameters $A = 1$, $\sigma = 1$.

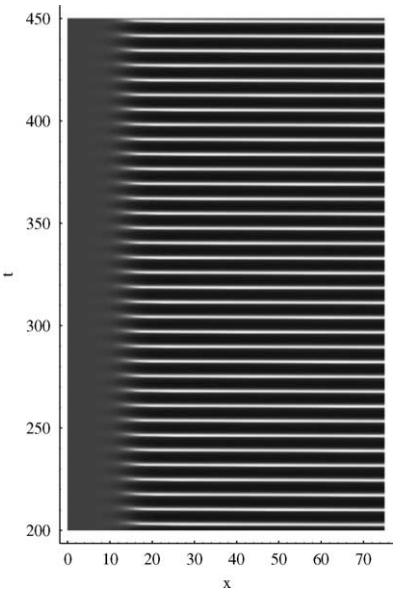

Fig. 2. Spatio-temporal diagram for the system (2). The gray scale represents U: lighter tones correspond to larger values. The parameters are $A = 1$, $B = 3$, $\sigma = 1$, and $v = 1.35$ ($v_{ca} \approx 1.414$, $v_{st} \approx 1.225$) that correspond to the domain II in Fig. 1. The inflow perturbation is absent, i.e, $U_{in} = V_{in} = 0$. The absolute Hopf instability develops in this case.

In the domain IV, the FDS solution decays near the inlet and the Hopf mode is convectively unstable. This results in the decaying of the perturbation to the steady state in every fixed point.

3. Spatio-temporal diagrams and description of the FDS-Hopf competition

To investigate the competition, we find the solutions to the system (2) numerically using the semi-implicit finite difference method of the second order (Cranck–Nicholson scheme) with the time and space steps about 0.1. The

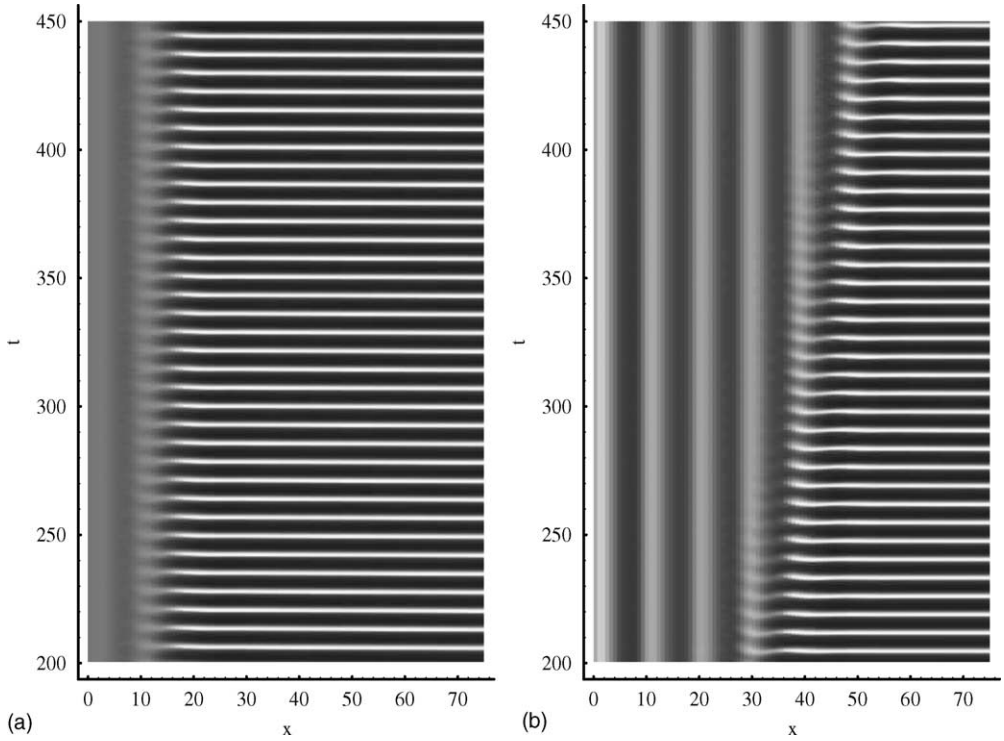

Fig. 3. Rigid transition to FDS in the Brusselator model (2). The parameters are the same as in Fig. 2, but now the inflow boundary is nonhomogeneous. The inflow perturbation in panel (a) is $U_{\text{in}} = 0.05$ that is small to grow to FDS and the Hopf mode spreads over space. Larger perturbation $U_{\text{in}} = 0.5$ in panel (b) results in the rigid transition to FDS and in the imposed convective Hopf instability.

inlet boundary conditions are

$$U(x,t)_{|x=0} = U_{\text{S}} + U_{\text{in}}, \quad V(x,t)_{|x=0} = V_{\text{S}} + V_{\text{in}}, \tag{7}$$

where $(U_{\text{S}}, V_{\text{S}})$ is the homogeneous steady state (3), and $(U_{\text{in}}, V_{\text{in}})$ is the constant perturbation. At the outlet, as usual for systems of considered type, the zero flux boundary conditions are applied.

Fig. 2 presents the numerical solution to Eq. (2) in the domain II when the inflow perturbation is absent, i.e. when $U_{\text{in}} = V_{\text{in}} = 0$. The Hopf instability is absolute in this domain. The homogeneous oscillations occupies almost the whole area of the reactor except the narrow boundary layer where the oscillations attain their limit amplitude.

Fig. 3 illustrates the case when the constant perturbation is applied at the inflow boundary. In panel (a), the perturbation is sufficiently small and decays right near the inlet. Observe that the sizes of the boundary layers in this case and in the case of the homogeneous boundary, Fig. 3, are identical. The increasing of the perturbation changes the picture and results in the rigid transition to FDS. In panel (b), the large inflow perturbation grows in space and develops into the FDS. The Hopf mode becomes convectively unstable, and the boundary between FDS and Hopf domains moves downstream. This will be referred to as an imposed convective instability.

The rigid transition to FDS exist only if the flow rate is sufficiently high. This is illustrated in Fig. 4 where the flow rate is a little bit smaller. In panel (a) of this figure, the inflow perturbation is small and this decays as in the previous figure. Large perturbation in panel (b) grows to the FDS but now this does not produce the imposed convective instability. The boundary between FDS and Hopf domains remains in a fixed position, and two these solutions coexist.

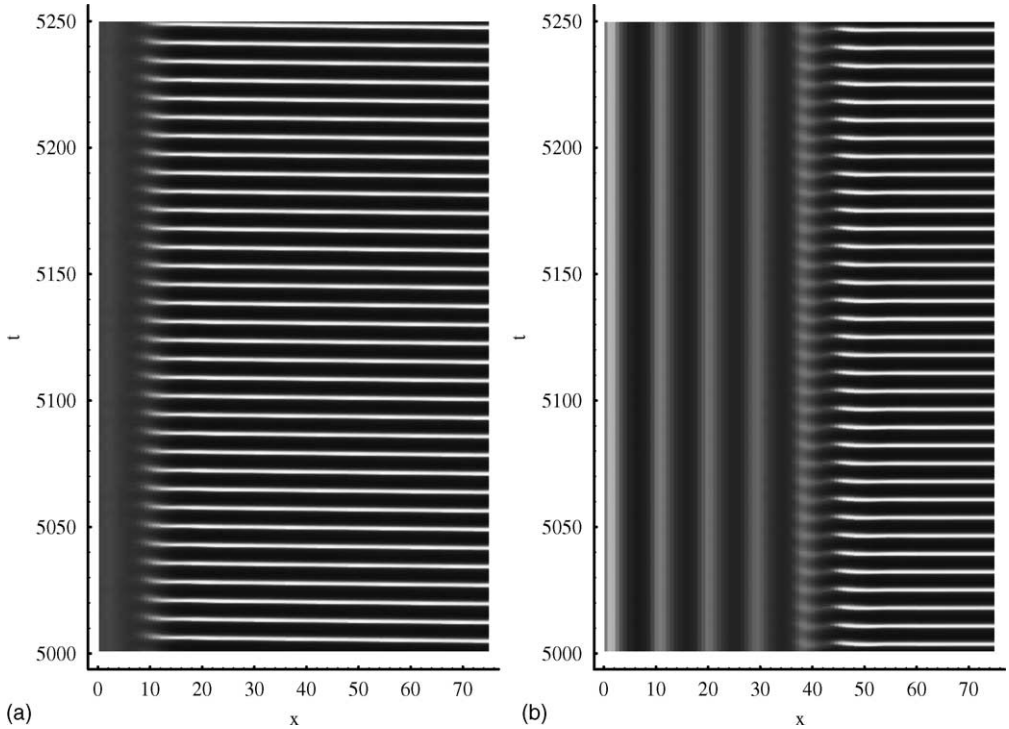

Fig. 4. Same as Fig. 3, but for smaller flow rate $v = 1.3$. In panel (a), the inflow perturbation is small to grow to the FDS. In panel (b), the inflow perturbation is large and the FDS solution though appears but does not expand. The FDS and Hopf solutions coexist.

Further decreasing of the flow rate is illustrated in Fig. 5. First, the FDS domain becomes more narrow, as seen from panel (a). When the flow rate is very small, see panel (b), the FDS vanishes and even very large inflow perturbation decays.

The figures presented above are obtained in the vicinity of the left boundary of the domain II in Fig. 1. Increasing the parameter B, we observe that the effect of the rigid transition to FDS survives. Fig. 6 shows how small inflow perturbation decays, while the large one grows to the FDS. However, the flow rate band where the FDS and Hopf solutions coexist shrinks. The effect of coexistence is obtained in Fig. 7(a) for $v = 1.414$, and even small variation of the flow rate destructs this. Fig. 7(b) shows the vanish of the FDS domain already for $v = 1.413$, and a little bit larger flow rate in Fig. 6, $v = 1.416$, results in the appearance of the rigid transition to the FDS. If the parameter B grows further, effect of coexistence becomes rather unobservable.

Finally, in Fig. 8 we present the examples of the discussed phenomenology when the diffusion rates of the reacting species U and V are different. In panel (a), the large inflow perturbation at the high flow rate produces the rigid transition to FDS and the imposed convective instability (as in Fig. 3(b)). In panel (b), the small flow rate does not results in the imposed convective instability even at the large inflow perturbation, and the FDS and Hopf solutions coexist (compare with Fig. 4(b)).

Thus, we observe that the result of the FDS-Hopf competition in the neighborhood of the inlet is determined by the inflow perturbation: the small perturbation decays, while the large one can grow. In the former case further development of the competition depends on the flow rate. Increasing of the inflow perturbation when the flow rate is large gives rise the rigid transition to FDS and the imposed convective Hopf instability. Small flow rate together with the large perturbation results in the coexistence of the FDS and Hopf solutions. This is observed until the flow rate is sufficiently large. Decreasing of the flow rate, we observe the shrinking of the FDS domain, and, finally,

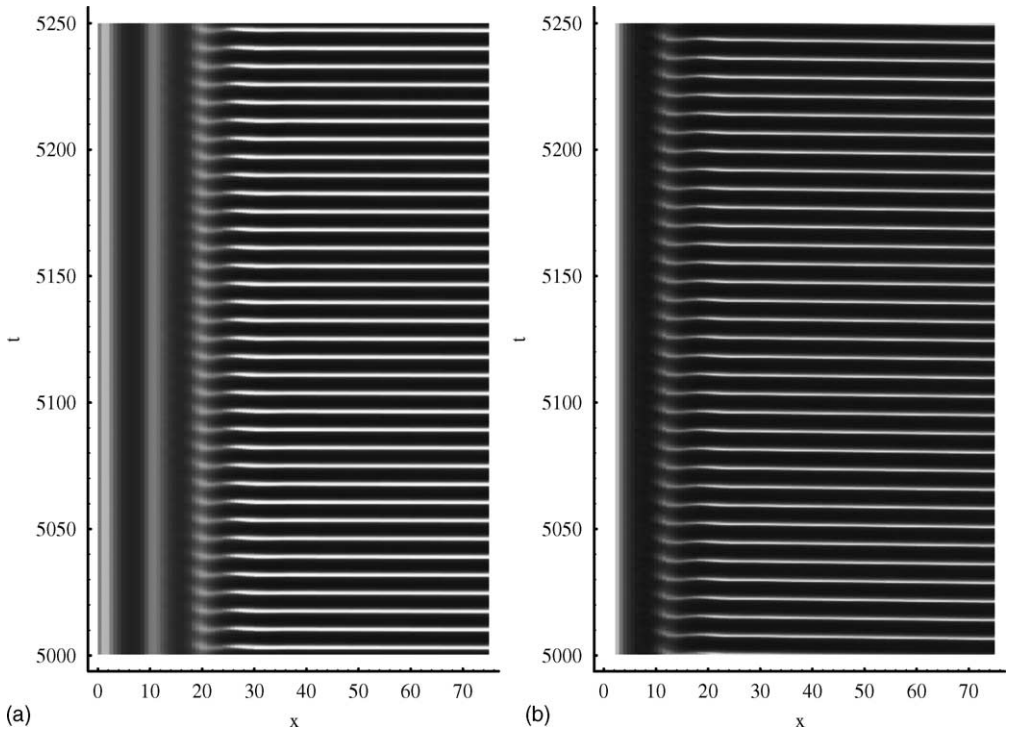

Fig. 5. Further decreasing of the flow rate: (a) $v = 1.27$, $U_{\text{in}} = 0.5$; (b) $v = 1.23$, $U_{\text{in}} = 5$. In panel (a) reducing of the flow rate results in the shrink of the FDS domain (compare with Fig. 4(b)). When the flow rate becomes very small, as in panel (b), the FDS vanishes right near the inlet. Notice that this takes place even if the inflow perturbation is very large.

the FDS domain disappears. Coexistence of the FDS and Hopf solutions is easier to observe for sufficiently small parameter B, while increasing of B reduces the flow rate band where this effect is observable.

4. Discussion

4.1. Stepwise propagation of the FDS-Hopf boundary

Specific feature of the presented spatio-temporal diagrams is the stepwise propagation of the FDS-Hopf domain boundary. (The interaction between forming FDS pattern and oscillating solution was observed in several experiments [23,21].) As seen from Figs. 3(b), 6(b), and 8(a), the boundary spends sufficiently long time near the minima of U_{FDS} (the dark vertical stripes in the figures) and jumps very fast from one minimum to another. This is seen more clearly from Fig. 9 which shows the trajectory of the domain boundary and positions of the minima of U_{FDS}. Because the FDS solution does not depend on time, the position of the FDS-Hopf boundary is found in this figure as the point where $|\partial U/\partial t|$ attains 0.01 for the the first time (0.01 is an arbitrary small value). Panel (a) of Fig. 9 presents the imposed convective instability at high flow rate and at large inflow perturbation. The trajectory of the domain boundary looks like a staircase: the boundary moves slowly near the minima of U_{FDS} (dashed vertical lines in the figure) and runs very fast being close to the maxima. Panel (b) shows the trajectory when the flow rate is small and does not produce the imposed convective instability. The stepwise slowing-down of the boundary is observed. Every successive minimum holds the domain boundary longer than the previous one, and, finally, the boundary stops.

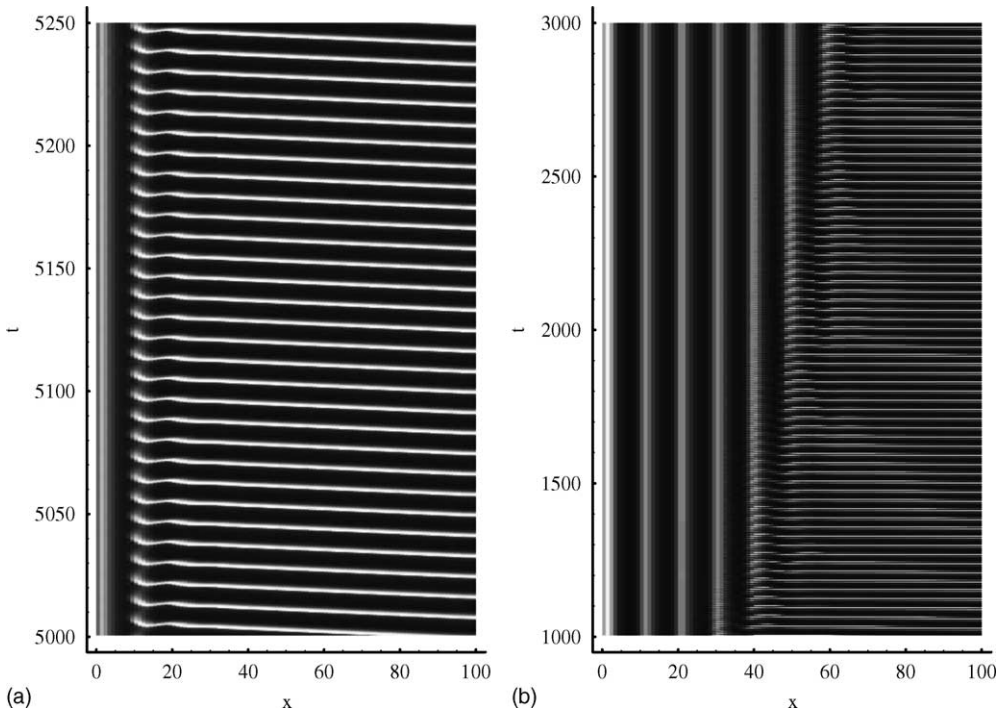

Fig. 6. Rigid transition to FDS for a larger value of the parameter B: $A = 1$, $B = 3.3$, $\sigma = 1$, and $v = 1.416$ ($v_{ca} \approx 1.612$, $v_{st} \approx 0.943$). Such a specific value of v is taken just to compare this figure with the next one, and the effect remains observable for any larger flow rate that falls below the critical value v_{ca}. In panel (a), the inflow perturbation $U_{in} = 0.5$ is insufficient to grow, while in panel (b), lager perturbation $U_{in} = 1$ produces the FDS and the imposed convective instability. (Notice that the original Hopf structure is not seen in panel (b) because the large time interval is taken.)

Let us consider some point near the FDS-Hopf domain boundary. In the small vicinity of this point the dynamics can be treated as a Hopf oscillations near the steady state (U_{FDS}, V_{FDS}). Locally, these oscillations may be described by the Brusselator equation where the actual control parameters A and B are substituted with the values A_{loc} and B_{loc}. These local control parameters can be found from Eq. (3) as $A_{loc} = U_{FDS}$, $B_{loc} = U_{FDS} V_{FDS}$. The bifurcation point for the Hopf oscillations is now $1 + A_{loc}^2$. This value is, obviously, large in the maxima of U_{FDS} and small in the minima. There is no simple estimation for B_{loc}, but from the mentioned above figures we can assume that it have the opposite phase: B_{loc} is large in the minima of U_{FDS} and small in the maxima. Therefore, fast decaying of the Hopf oscillations in the maxima of U_{FDS} takes place because B_{loc} is far below the bifurcation point $1 + A_{loc}^2$. As a result, the FDS-Hopf domain boundary runs over these points very fast. On the contrary, in the minima the distance from the bifurcation point is small, and this manifests itself as a long staying of the domain boundary near these points. If $B_{loc} < 1 + A_{loc}^2$ in every point, the imposed convective instability takes place as in Fig. 9(a). But if B_{loc} in the minima of U_{FDS} falls above the critical point, the domain boundary stops and the imposed convective instability disappears as in Fig. 9(b).

4.2. Imposed convective instability

Let us now discuss in more details the transition to the imposed convective instability. In this analysis and below, we shall assume that $\sigma = 1$.

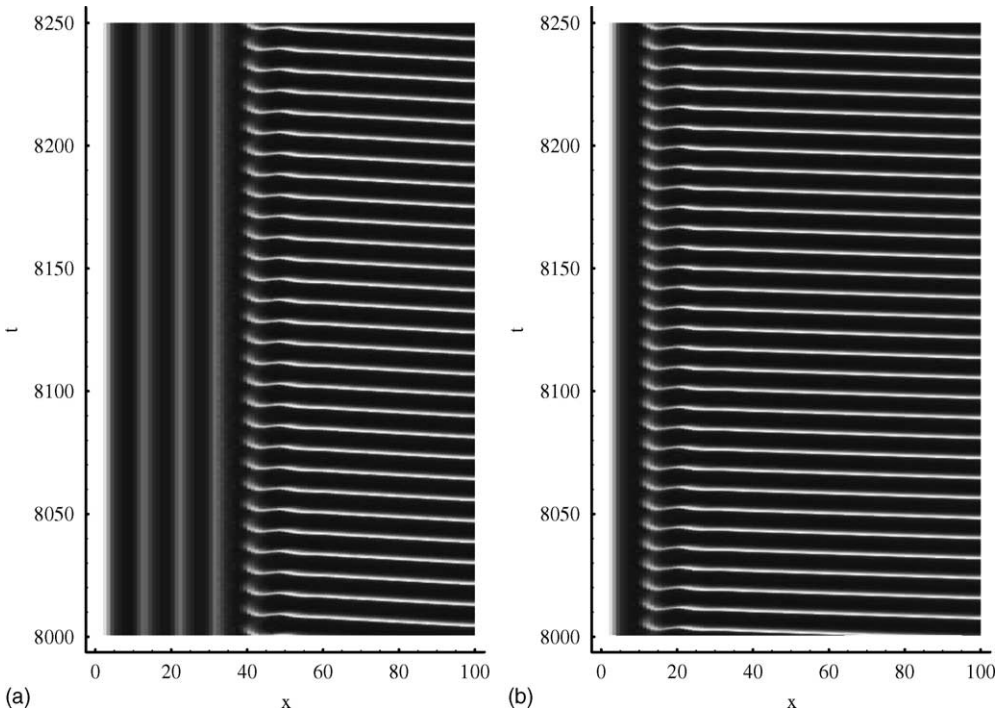

Fig. 7. Same as Fig. 6, but for $v = 1.414$ in panel (a) and $v = 1.413$ in panel (b). For both panels $U_{\text{in}} = 5$. The effect of coexistence of the FDS and Hopf solutions in panel (a) emerges now in the very narrow band of the flow rates. Small increment of the flow rate results in the appearance of the rigid transition to FDS and the imposed convective instability, as in Fig. 6(b), while the small decrement results in the vanish of the FDS domain, as shows panel (b).

It is natural to suppose that the imposed convective instability takes place if the amplitude of FDS exceeds some critical value α_{imp}. To find α_{imp}, we use the following ansatz for the solution to Eq. (2):

$$U(x,t) \to \alpha\, U_{\text{FDS}}(x) + U(x,t), \qquad V(x,t) \to \alpha\, V_{\text{FDS}}(x) + V(x,t). \tag{8}$$

$U(x,t)$ and $V(x,t)$ in the right part denote the Hopf solution that should be determined. $U_{\text{FDS}}(x)$ and V_{FDS} are the sinusoidal functions with the periods and phases as the actual FDS solution and with the amplitudes controlled by the parameter α. We determine $U_{\text{FDS}}(x)$ and V_{FDS} form the stationary solution to the linearized Eq. (2) neglecting the real parts of the complex conjugated eigenvalues:

$$U_{\text{FDS}}(x) = \tfrac{1}{2} K_U \mathrm{e}^{\mathrm{i}\Lambda x} + \text{c.c.}, \qquad V_{\text{FDS}}(x) = \tfrac{1}{2} K_V \mathrm{e}^{\mathrm{i}\Lambda x} + \text{c.c.}, \tag{9}$$

where "c.c." denote the complex conjugated terms, Λ is the real wave number (equation for Λ is not written here because Λ does not appear in the resulting equations), and (K_U, K_V) is the eigenvector

$$K_U = 1, \qquad K_V = \frac{1 - A^2 - B + \sqrt{(1 + A^2 - B)^2 - 4A^2}}{2A^2}. \tag{10}$$

Notice that because $K_U = 1$, α is, in fact, the amplitude of the component U. Because we are searching for the Hopf solution, we can suppose that $U(x,t)$ and $V(x,t)$ vary in space much slower than $U_{\text{FDS}}(x)$ and $V_{\text{FDS}}(x)$. Thus, after the substitution (8), we can average Eq. (2) over the period of FDS treating $U(x,t)$ and $V(x,t)$ as constants. As a result, we obtain the set of equations without the explicit dependence on x. After linearization and decomposition

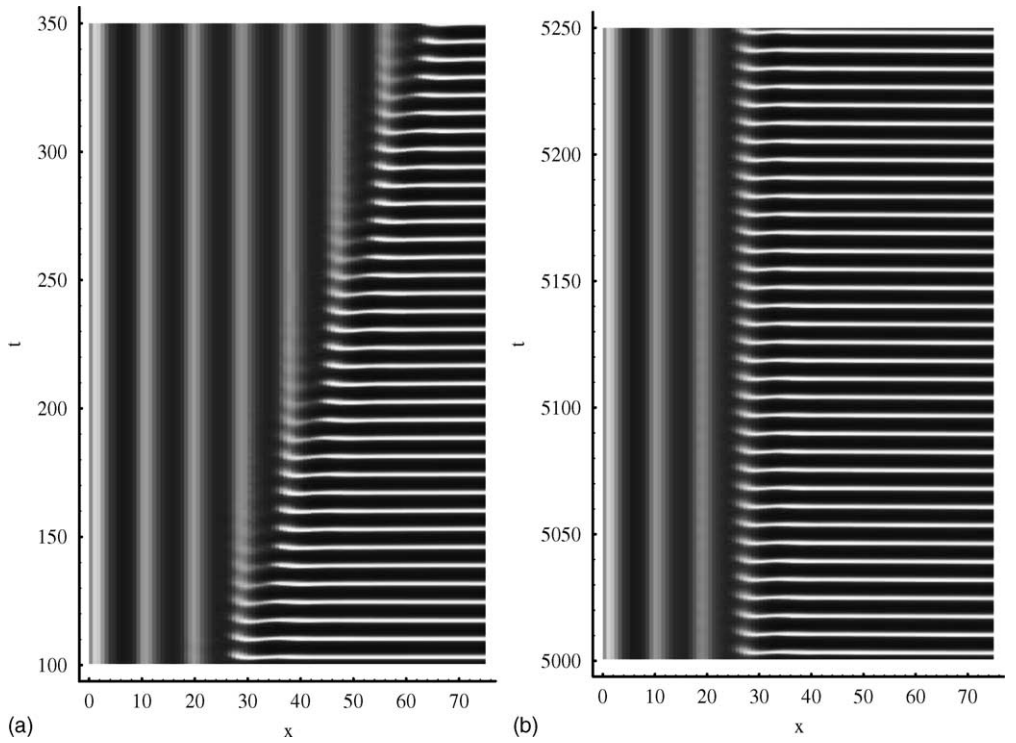

Fig. 8. Examples of the rigid transition to FDS and the FDS-Hopf coexistence for $\sigma = 0.8$ ($v_{ca} \approx 1.361$, $v_{st} \approx 1.022$). The other parameters are as in Figs. 3 and 4. In both panels, $U_{in} = 0.5$. In panel (a), $v = 1.2$, and the FDS invades the space. In panel (b), $v = 1.1$. The FDS-Hopf domain boundary stays in a fixed position, and two solutions coexist.

over the elementary waves e^{st+qx}, we obtain the dispersion equation:

$$d(s,q) = A^2 + (v\,q - q^2 + s)^2 + \frac{\alpha^2}{2} + (v\,q - q^2 + s)\left(3 - A^2 - B + \alpha^2 + \frac{\alpha^2(B-1)}{2A^2} + \frac{4(A^4 - A^2)}{2A^2 + \alpha^2}\right). \tag{11}$$

In absence of FDS at $\alpha = 0$, this equation coincides with the dispersion equation for the Brusselator with flow (4). Thus, we have the well known problem of transition from absolute to convective instability, but, unlike the ordinary case, now the flow rate is known, and α should be determined. To find the critical amplitude $\alpha = \alpha_{imp}$, we solve Eqs. (11) and (1) numerically. From these equations we obtain that $\alpha_{imp} = 0$ for $v = v_{ca}$, and α_{imp} grows when v decreases. This is shown in Fig. 10.

4.3. Critical inflow perturbation

It is interesting to compare the theoretical value α_{imp} with the critical inflow perturbation α_{rig} for which the rigid transition to FDS takes place. To find α_{rig}, we set the left boundary condition as

$$U_{in} = U_S + \alpha\, U_{FDS}(0), \qquad V_{in} = V_S + \alpha\, V_{FDS}(0), \tag{12}$$

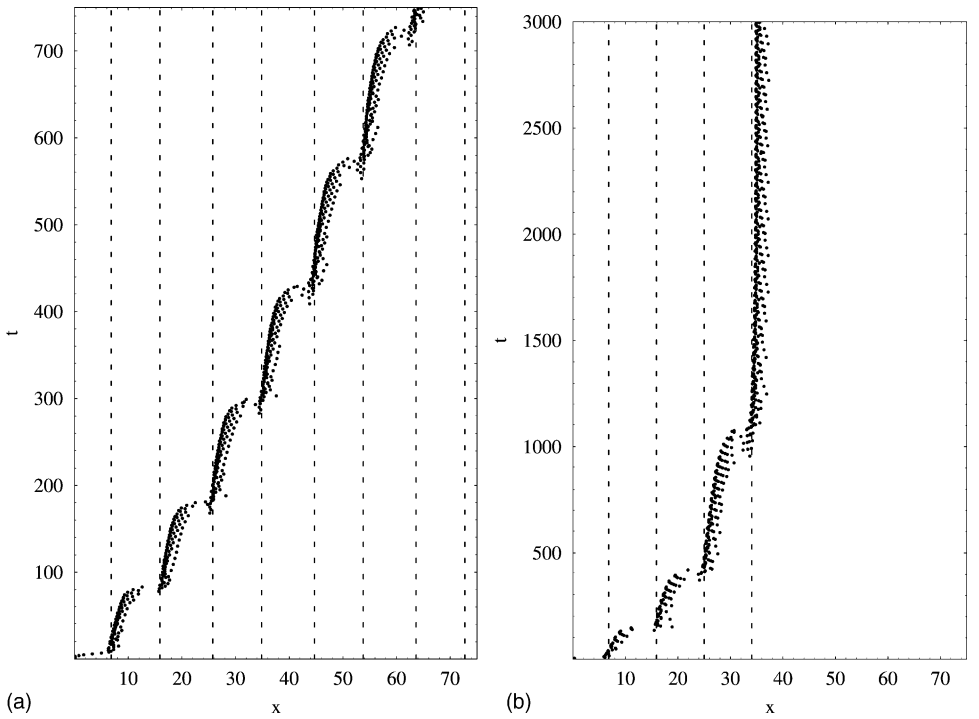

Fig. 9. Trajectory of the boundary between the FDS and Hopf domains. The boundary is founded as a point where $|\partial U/\partial t|$ exceeds 0.01 for the first time. The parameters in panels (a) and (b) are as in Fig. 3(b) and 4(b), respectively. In panel (a), the flow rate is large, and the FDS expands. In panel (b), the flow rate is small, and the domain boundary tends to a fixed position. The vertical dashed lines mark the minima of U_{FDS}. Notice the staircase structure of the trajectory: the boundary moves slowly near the minimum for some time, then jumps over the FDS period, and moves slowly again near the next minimum.

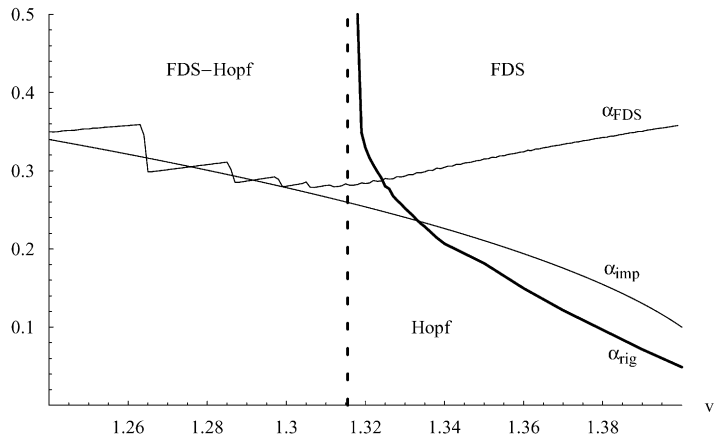

Fig. 10. Critical inflow perturbation α_{rig} for the rigid transition to FDS, critical amplitude of FDS α_{imp} for the imposed convective Hopf instability, and amplitude of FDS α_{FDS} near the domain boundary. α_{imp} is the numerical solution to Eqs. (11) and (1). α_{rig} and α_{FDS} are obtained directly from the numerical solutions to Eqs. (2). The vertical asymptotic line for curve α_{rig} separates the regions where the rigid transition to the FDS takes place and where the FDS and Hopf solutions coexist. The parameters are $A = 1$, $B = 3$, and $\sigma = 1$.

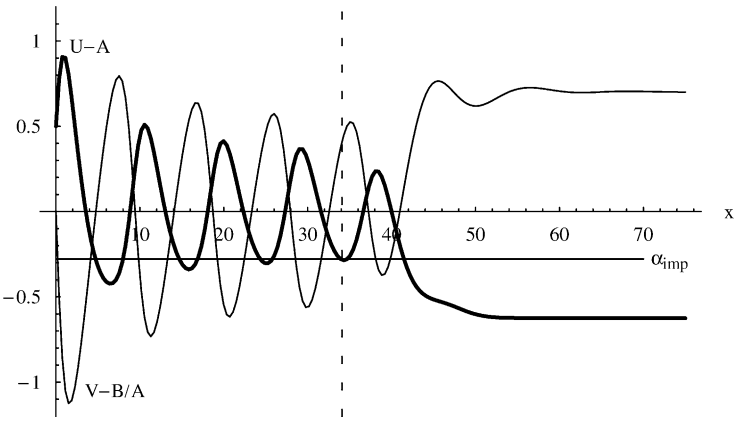

Fig. 11. Distribution of U and V in the fixed time moment (after the large transient time) when the flow rate is small and the inflow perturbation is large, i.e., when the FDS and Hopf solutions coexist. The parameters are as in Fig. 4(b). Dashed vertical line separates the FDS and Hopf domains. This domain boundary is found as in Fig. 9(b). Solid horizontal line marks the critical amplitude for the imposed convective instability α_{imp}. Observe that the inflow perturbation is larger then α_{imp} and the FDS amplitude (we define it as an amplitude of U) decays until attains α_{imp}. It is this point where the domain boundary is located.

where U_{FDS} and V_{FDS} are given by Eq. (9). Then we solve Eq. (2) numerically at different α waiting for jumps of the domain boundary from one minimum of U_{FDS} to another. If at last four jumps are recorded during the observation time, we decide that $\alpha > \alpha_{rig}$ while the less number of jumps are treated as the approaching to the fixed position at $\alpha < \alpha_{rig}$. Using the bisection we find α_{rig} with required precision.

The actual precision of our computations is sufficiently low because described direct method works very slow. For every α the numerical solution to the system (2) should be found for a very long time before we can come to a conclusion, wether α is above the critical point or not.

Fig. 10 shows the dependence of α_{rig} on the flow rate. α_{rig} grows with decreasing of the flow rate and diverges. This curve and its vertical asymptotic line (dashed line in the figure) split the plane onto three regions. To the right of the asymptotic line and below the curve α_{rig} the Hopf solution occupies the whole space, as in Fig. 3(a). Above this curve the rigid transition to the FDS takes place. In this region, the FDS expands and produces the imposed convective Hopf instability, as illustrated in Figs. 3(b) and 8(a). To the left of the asymptotic line sufficiently large

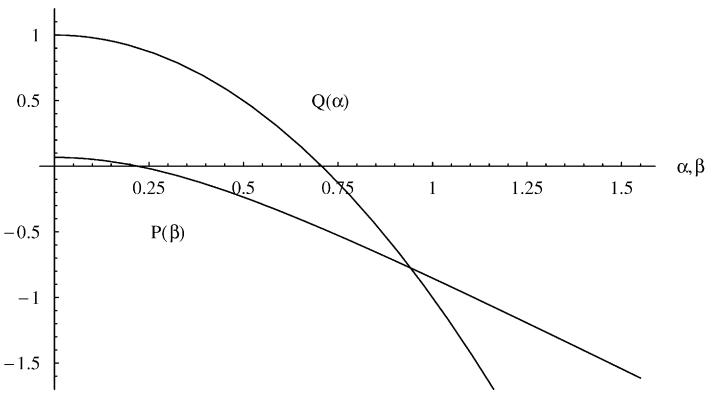

Fig. 12. Hopf increment $Q(\alpha)$, Eq. (14), and FDS increment $P(\beta)$, Eq. (19), for $A = 1$, $B = 3$, $v = 1.35$. The FDS-Hopf competition takes place when α and β are inside their bands of competition where $Q(\alpha) > 0$ and $P(\beta) > 0$ simultaneously. Notice that the FDS amplitude α has larger band of competition. Hence, to win the competition, it should have sufficiently large initial value.

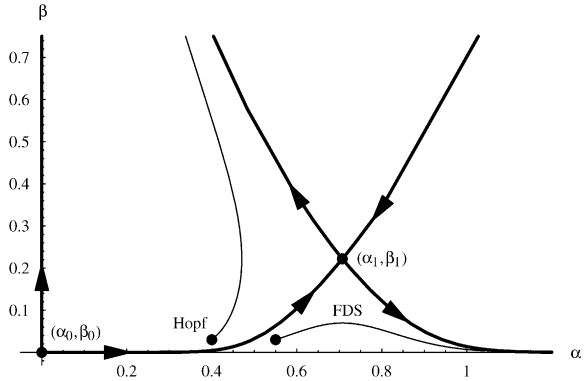

Fig. 13. Phase plane for the competition equations (23). (α_0, β_0) and (α_1, β_1) are the fixed points. The arrowed curves are their stable and unstable manifolds. The fixed points are joined by the heteroclinic orbit. Two thin curves starting from the bullet points are the trajectories that illustrate the cases when either the Hopf solution or the FDS solution wins the competition. Notice how result of the competition depends on the position of the initial point relatively to the heteroclinic orbit. The parameters are $A = 1$, $B = 3$, $v = 1.35$.

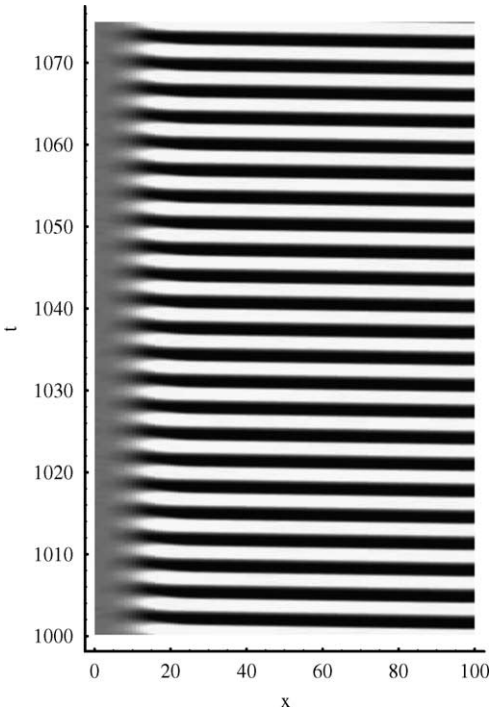

Fig. 14. Absolute Hopf instability in the Lengyel–Epstein model (A.1). $a = 11$, $b = 0.5$, $c = 1.5$, $\delta = 5$, $\phi = 0.8$. The inflow perturbation is absent, $U_{\text{in}} = V_{\text{in}} = 0$.

inflow perturbation produces the limited FDS domain near the inlet. The FDS and Hopf solutions coexist, and the FDS-Hopf domain boundary stays in a fixed position. This case is illustrated in Figs. 4 and 8(b).

Observe that curves α_{rig} and α_{imp} in Fig. 10 behave different. It means that the rigid transition to FDS can not be deduced just from the imposed convective instability and contains at leats two stages. The first one happens near the inlet, and its result depends on the inflow perturbation. If the perturbation is higher than α_{rig}, the FDS suppresses the

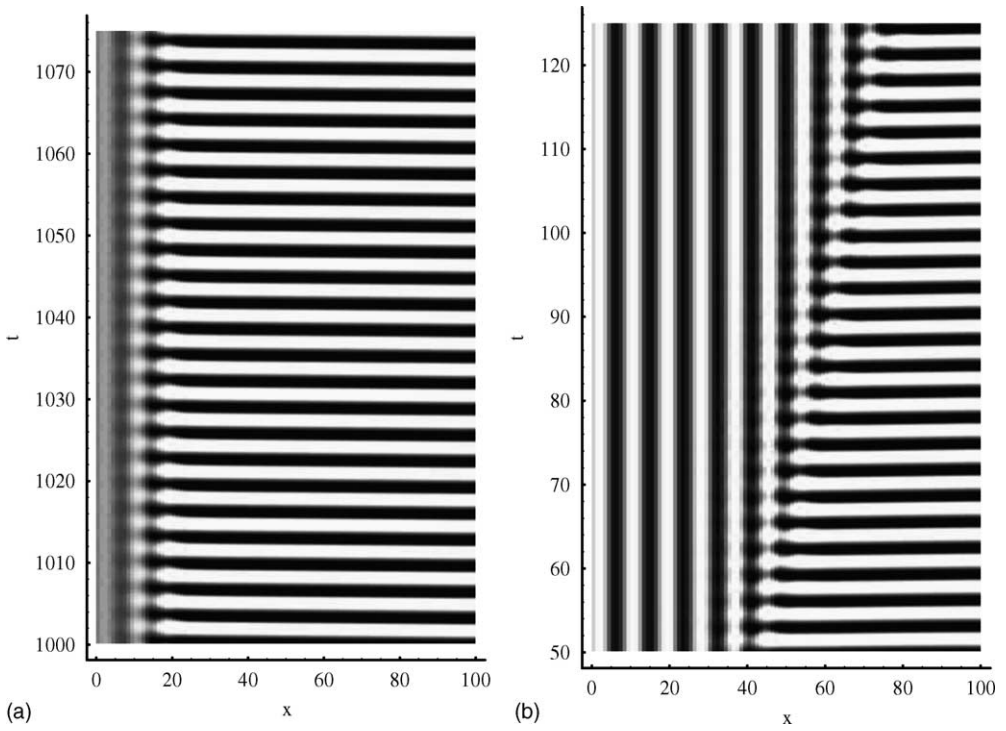

Fig. 15. Rigid transition to the FDS in the Lengyel–Epstein model (A.1). The parameter are similar to Fig. 14. In panel (a), the inflow perturbation $U_{\text{in}} = 0.1$ is insufficient to develop into the FDS, while in panel (b), large inflow perturbation $U_{\text{in}} = 0.5$ grows and produces the imposed convective Hopf instability.

Hopf oscillations. Notice that at large flow rate the critical inflow perturbation α_{rig} is smaller than the critical FDS amplitude α_{imp}, while near the asymptotic line α_{rig} is much more larger than α_{imp}. On the second stage the FDS solution attains the stationary amplitude, and, if this is larger than the critical value α_{imp}, the imposed convective instability takes place, as observed to the right of the asymptotic line in Fig. 10.

4.4. FDS amplitude

Let α_{FDS} denotes the amplitude of FDS near the domain boundary. We define this as the amplitude of the component U and obtain directly from the numerical solutions to Eq. (2). The measurement of this value is performed at different flow rates for the fixed inflow perturbation (12) where α is taken being large enough for FDS to grow.[1] After a large transient time we find the position of the domain boundary, then search the nearest minimum of U_{FDS} (this can be found to the left or to the right from the boundary), and, finally, measure the amplitude in this point as $U - U_{\text{S}}$. Performing this procedure for several successive time steps, we average the measurements and obtain the resulting FDS amplitude α_{FDS}.

Fig. 10 shows the dependence of α_{FDS} on the flow rate. As we expected, in the right part of this figure the amplitude of FDS is always larger than the critical amplitude α_{imp}. This is responsible for the emergence of the imposed convective instability.

[1] α_{FDS} is rather insensible to the choice of α. In Fig. 10 $\alpha = 2$ for $v \leq 1.34$ and $\alpha = 0.5$ for $v > 1.34$. Observe that there is no breakup at $v = 1.34$.

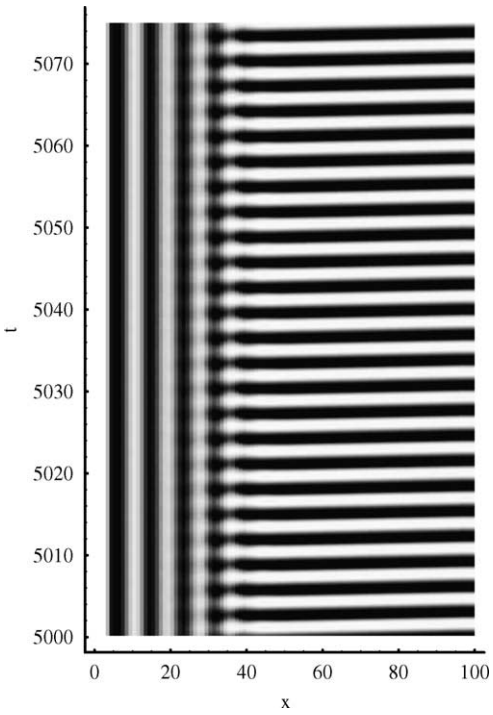

Fig. 16. Coexistence of the FDS and Hopf solutions in the Lengyel–Epstein model (A.1). The flow rate $\phi = 0.72$ is insufficient for the imposed convective instability to take place. Large inflow perturbation $U_{\text{in}} = 2$, however, develops into the localized FDS domain near the inlet. All other parameters are as in Fig. 14.

In the right part of the plane in Fig. 10, the amplitude of FDS decreases with decreasing of the flow rate. To explain this, we should take into account that the formation of the FDS is determined by two opposite influences. The kinetics of the system is responsible for the growth of the inflow perturbation to the periodic structure, while the diffusion tends to flatten the spatial inhomogeneity. The FDS with a small period is more inhomogeneous than this having a large period. As known [11,12], the FDS period is proportional to the flow rate. Thus, when the flow rate decreases, the action of the diffusion becomes more intensive and, hence, the amplitude of the FDS becomes smaller.

In the left part of Fig. 10, the FDS amplitude becomes smaller than the critical value α_{imp} and the imposed convective Hopf instability disappears. But if the inflow perturbation (12) is such that $\alpha > \alpha_{\text{imp}}$ the FDS, while relaxing, produces the local imposed convective instability. The domain boundary moves until the FDS amplitude remains above the critical value. This is illustrated in Fig. 11. As seen, the domain boundary has attained the point where the FDS amplitude is equal to α_{imp}. (Notice also that in the left part of Fig. 10 α_{FDS} is equal to α_{imp} at the average.) This results in the formation of a localized domain of the FDS near the inlet. This case is illustrated in Figs. 4(b) and 8(b).

The curve $\alpha_{\text{FDS}}(v)$ in the left part of Fig. 10 has a stepwise structure. Every growing segment of this curve corresponds to the staying of the FDS-Hopf boundary near one of the minima of U_{FDS}, and shows the growth of the amplitude in this point. This minimum is the last one with the amplitude that is larger than α_{imp}. The jump to the next minimum (and emergence of the subsequent segment of the curve) happens when its amplitude becomes enough to produce the imposed convective instability. Observe that the slopes of the segments are similar to the slope of the curve $\alpha_{\text{FDS}}(v)$ in the right part of the figure.

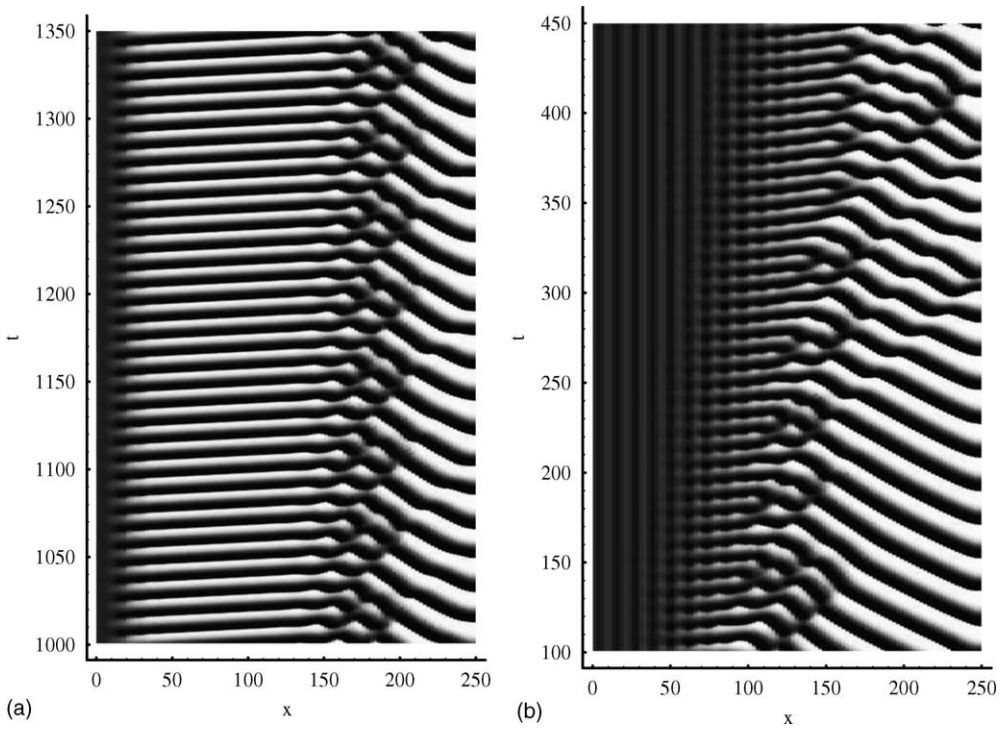

Fig. 17. Rigid transition to FDS for the system (A.2). $p = 0.2$, $\delta = 5$, $\mu = 0.7$, $\phi = 0.3$. (a) The inflow perturbation $U_{\text{in}} = 0.01$ is small. (b) The inflow perturbation $U_{\text{in}} = 0.05$ is sufficient for the rigid transition.

As we discussed above, see Fig. 5, decreasing of the flow rate results in the shrink and vanish of the FDS domain. For sufficiently small flow rate even very large inflow perturbation does not produce the local imposed convective instability. This takes place because the stationary FDS amplitude (i.e., the amplitude which could be attained in absence of the Hopf oscillations) is much smaller than α_{imp}. The inflow perturbation decays very fast right near the inlet, and the FDS domain does not appear.

4.5. Amplitude equations for the FDS-Hopf competition

Let us now analyze the competition between the FDS and Hopf solutions near the inlet after a short time of evolution. We assume again that $\sigma = 1$.

Let α be the amplitude of the FDS solution, and β denotes the Hopf amplitude. First, we suppose that the FDS exists in the system and find the condition for the Hopf instability. The following ansatz is used:

$$U(x,t) \to \alpha\, U_{\text{FDS}}(x) + U(t), \qquad V(x,t) \to \alpha\, V_{\text{FDS}}(x) + V(t), \tag{13}$$

where in the right part the functions $U_{\text{FDS}}(x)$ and $V_{\text{FDS}}(x)$ are the sinusoidal approximation (9) of the FDS solution, α is the FDS amplitude, and $U(t)$ and $V(t)$ denote the Hopf solution that should be determined. After substitution (13) to (2) and averaging over the FDS period, we linearize the equation near the steady state and obtain the set of two linear ordinary differential equations for $U(t)$ and $V(t)$. Two eigenvalues of these equations are complex conjugated and their the real part is

$$Q(\alpha) = -3 + A^2 + B + \frac{1 - 2A^2 - B}{2A^2}\alpha^2 + \frac{4A^2(1 - A^2)}{2A^2 + \alpha^2}. \tag{14}$$

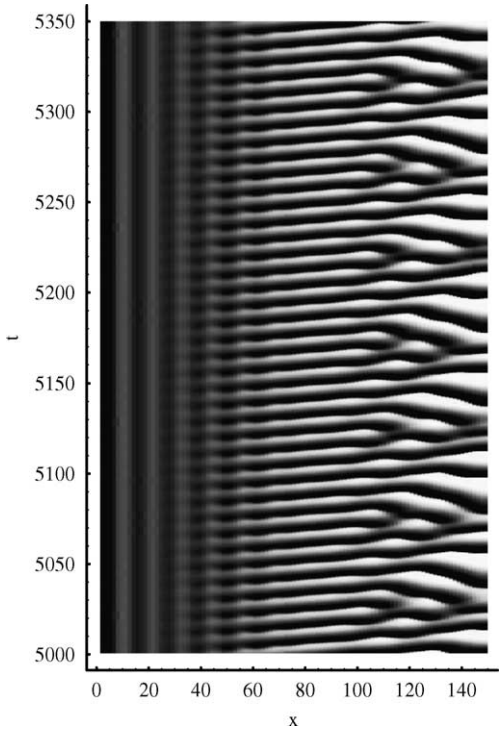

Fig. 18. Coexistence of the FDS and Hopf solutions in the system (A.2). $\phi = 0.25$, $U_{\text{in}} = 2$. The other parameters are the same as in Fig. 17.

Thus, the temporal growth (or decaying) of the Hopf solution $(U(t), V(t))$ can be estimated as

$$U(t), V(t) \propto \exp(Q(\alpha)t). \tag{15}$$

Hence, we can write the following equation for the Hopf amplitude β:

$$\frac{\partial \beta}{\partial t} = Q(\alpha)\beta. \tag{16}$$

Notice that in this equation α is treated as the control parameter, and β is the dynamical variable depending on t.

Similarly, we can obtain the equation for the FDS amplitude α controlled by the Hopf amplitude β. Let us suppose that the Hopf solution presents in the system. As well as for the FDS solution, we do not know the exact Hopf solution and use the sinusoidal approximation instead:

$$U_{\text{H}}(t) = \tfrac{1}{2} K_U e^{i\Omega t} + \text{c.c.}, \qquad V_{\text{H}}(t) = \tfrac{1}{2} K_V e^{i\Omega t} + \text{c.c.}, \tag{17}$$

where Ω is the Hopf frequency, and K_U and K_V are given by Eq. (10). To find the condition for the FDS instability on the Hopf background, we use the ansatz

$$U(x, t) \to \beta\, U_{\text{H}}(t) + U(x), \qquad V(x, t) \to \beta\, V_{\text{H}}(t) + V(x), \tag{18}$$

where β is now the constant control parameter, and $(U(x), V(x))$ is the FDS solution that should be determined. Substituting the ansatz to Eq. (2), then averaging, and, finally, linearizing near the steady state, we find that the

linear increment for $U(x)$ and $V(x)$ is

$$P(\beta) = v - \frac{\sqrt{R_+} + \sqrt{R_-}}{4A^2 + 2\beta^2}, \tag{19}$$

where

$$R_\pm = 4A^4(2 + 2A^2 - 2B + v^2) \pm 2A^2\sqrt{R_0} + (4A^2(3 + 2A^2 - B + v^2) \pm \sqrt{R_0})\beta^2 + (2 + 6A^2 + 2B + v^2)\beta^4 + \left(\frac{(-1 + 2A^2 + B)}{A^2}\right)\beta^6, \tag{20}$$

$$R_0 = 16A^4(A^4 + (B-1)^2 - 2A^2(B+1)) + 16A^2(2 + A^4 - 2B - A^2(B+3))\beta^2 + 4(2 + 5A^4 - 2(B-2)B - 2A^2(B+3))\beta^4 + \left(\frac{4(-2 + A^2 + 2A^4 + (2 + A^2)B)}{A^2}\right)\beta^6 + \left(\frac{(-1 + 2A^2 + B)^2}{A^4}\right)\beta^8, \tag{21}$$

Hence, we can write the equation for the FDS amplitude α as

$$\frac{\partial \alpha}{\partial x} = P(\beta)\alpha. \tag{22}$$

In this equation, α is the dynamical variable depending on x, and β is treated as the control parameter.

We have obtained two amplitude Eqs. (16) and (22). The first one describes the temporal evolution of the Hopf amplitude β, and the other one determines the spatial evolution of the FDS amplitude α. To describe the FDS-Hopf competition, we need to combine these equations into the equations set. A possible way is as follows. First, we suppose that α in Eq. (16) depends on x, and β in Eq. (22) depends on t. Then, we consider the dynamics of Eqs. (16) and (22) along the direction $x = t = \xi$ in the space-time coordinate plane. Thus, we can build the set of the amplitude equations describing the FDS-Hopf competition:

$$\frac{\partial \alpha}{\partial \xi} = P(\beta)\alpha, \qquad \frac{\partial \beta}{\partial \xi} = Q(\alpha)\beta. \tag{23}$$

Properties of the functions $Q(\alpha)$ and $P(\beta)$ determines the dynamics of the system (23). As seen form Eqs. (14) and (19) these functions are symmetric for the change of signs of their arguments, and, hence, we can consider only the positive values of α and β. When $\alpha = 0$, $Q(0)$ gives the condition for the Hopf instability. It easy to check that $Q(0) > 0$ if B is above the Hopf bifurcation point, i.e., $B > 1 + A^2$. Similarly, $P(0)$ is the FDS increment, and this is positive in the Hopf instability domain when $v > v_{st}$, see Eq. (6).

Functions $Q(\alpha)$ and $P(\beta)$ are plotted in Fig. 12. They are positive when their arguments are zeros, and decrease when α and β grow. Such behavior is responsible for the FDS-Hopf competition. When α and β are simultaneously inside their bands of competition, which are determined by the inequalities $Q(\alpha) > 0$ and $P(\beta) > 0$, the growth of one of the solutions results in the reduction of the increment of the other one and vice versa. If α leaves its band of competition first, $Q(\alpha)$ becomes negative while $P(\beta)$ is still positive. In this case, the FDS solution wins the competition. Its amplitude α diverges and β decays. Similarly, the Hopf solution wins if $P(\beta) < 0$ and $Q(\alpha) > 0$. Notice that the band of the competition for α is much larger than this band for β. It means that α have a chance to leave its band first if the initial value of α is much larger than the initial value of β.

The competition equations (23) have the fixed point $(\alpha_0, \beta_0) = (0, 0)$ and four fixed points $(\pm\alpha_1, \pm\beta_1)$, where α_1 is found from the equation $Q(\alpha_1) = 0$ and β_1 satisfies the equation $P(\beta_1) = 0$. Because of the symmetry of the functions $Q(\alpha)$ and $P(\beta)$, we shall consider only (α_0, β_0) and $(\alpha_1 > 0, \beta_1 > 0)$.

Linearization of Eq. (23) near (α_0, β_0) gives the eigenvalues and eigenvectors:

$$\Lambda_1 = P(0), \qquad \vec{\nu}_1 = (1, 0), \tag{24}$$

$$\Lambda_2 = Q(0), \qquad \vec{\nu}_2 = (0, 1). \tag{25}$$

At $v > v_{st}$ both eigenvalues are positive, hence, both eigendirections are unstable and (α_0, β_0) is an unstable node. The eigendirections of this node correspond to the unlimited growth of one of the variables while the other one is zero. If $v < v_{st}$, then $\Lambda_1 < 0$. In this case, (α_0, β_0) becomes the saddle whose stable manifold coincides with axis α. Only the Hopf solution can grow in this case.

For the second fixed point (α_1, β_1) we have:

$$\Lambda_1 = -\sqrt{\alpha_1\beta_1 Q'(\alpha_1)P'(\beta_1)}, \qquad \vec{\nu}_1 = \left(1, \quad \sqrt{\frac{\beta_1 Q'(\alpha_1)}{\alpha_1 P'(\beta_1)}}\right), \tag{26}$$

$$\Lambda_2 = \quad \sqrt{\alpha_1\beta_1 Q'(\alpha_1)P'(\beta_1)}, \qquad \vec{\nu}_2 = \left(1, -\sqrt{\frac{\beta_1 Q'(\alpha_1)}{\alpha_1 P'(\beta_1)}}\right), \tag{27}$$

where primes denote the derivatives. Because $Q'(\alpha_1) < 0$ and $P'(\beta_1) < 0$, the eigenvalues and the eigenvectors are real. The point (α_1, β_1) is the saddle when $v > v_{st}$. At $v < v_{st}$ the fixed point (α_1, β_1) disappears because $P(\beta)$ does not crosse zero.

Fig. 13 presents the phase plane for the competition Eq. (23) at $v > v_{st}$ (because of the symmetry only the first quarter is presented). The fixed points (α_0, β_0) and (α_1, β_1) as well as their manifolds are shown. The manifolds are obtained numerically via the Runge–Kutta method.

As seen from Fig. 13, there is the heteroclinic orbit in the phase plane that leaves (α_0, β_0) as the unstable manifold and attains (α_1, β_1) being the stable manifold of this point. This orbit plays the key role in the competition. If the staring point is above this orbit, the Hopf amplitude β grows while the FDS amplitude α decays. But if we start below the heteroclinic orbit, the FDS solution wins the competition.

The orbit is tangent to the axis α in the point (α_0, β_0) and, moreover, contains the large segment that passes asymptotically close to this axis. This determines the conditions for starting α (i.e., inflow perturbation in the original system (2)) and for β (initial conditions) that are required for the rigid transition to emerge: if starting β is small but finite, α should be sufficiently large to fall below the heteroclinic orbit. Notice that the critical value for the inflow perturbation depends on the initial β. For example, very small initial β permits the rigid transition for a sufficiently small inflow perturbation. This is the reason for a lot of troubles which, as noted above, we have met during the computation of α_{rig} for Fig. 10. Besides, this, probably, can be the source of difficulties in the experimental determination of the critical inflow perturbation for the rigid transition to FDS.

5. Manifestation of the rigid transition to FDS in experiments

Usually, an experimental setup for observation of FDS involves a tubular reactor that is fed from the outflow of a continually stirred tank reactor (CSTR) [12,21–23]. The state of the reaction medium in CSTR determines the boundary forcing at the tubular reactor inlet. This state is controlled by the residence time that, in turn, depends on the rate of pumping of reagents mixture into CSTR as well as on the rate of feeding them to the tubular reactor (the former is, in fact, the flow rate that is appears in the discussed reaction–diffusion equations). The CSTR is in an oscillatory state when the residence time is long and in a steady state when the residence time is short. The last one is the case of our interest.

The steady state of CSTR corresponds to the constant inflow perturbation of the tube reactor which can be varied by varying of the residence time. Thus, if the flow rate is varied without the keeping constant residence time, the value of

the inflow perturbation is varied too. In this case the rigid transition can confuse the interpretation of the experimental results. Indeed, the decreasing of the flow rate, on the one hand, may result in decreasing of the boundary perturbation, and, on the other hand, approaches the system to the critical point v_{st} where FDS solution disappears. If the system is in the soft transition domain, the decreasing of the inflow perturbation does not influence the formation of the FDS, and the FDS disappears only when the flow rate falls below the critical value v_{st}. But if the transition to FDS is rigid, the decreasing of the flow rate can make the inflow perturbation to be insufficiently large for the FDS to grow. As a result, the oscillating solution, that is absolutely unstable in the domain of rigid transition, starts to dominate over the FDS, and this is observed above the critical value v_{st}. This looks like a failure of the theoretic prediction.

Similar situation is reported in [23]. Here, the FDS pattern becomes unstable at the flow rate 0.08 sm/s instead of the expected 0.01 sm/s; furthermore, near the threshold point the competition is observed between the FDS and the oscillating solution which seems to be absolutely unstable. We guess that these observations can be interpreted as a manifestation of the rigid transition to FDS.

6. Conclusion

We considered the stationary flow and diffusion distributed structures (FDS) for the reaction–diffusion system with flow in the Hopf instability domain. The FDS is known to emerge when the constant inhomogeneous boundary condition is applied at the inlet and the Hopf mode is convectively unstable. In this paper, the FDS solution was considered when the Hopf mode was unstable absolutely. In this case, two solutions tend to invade the space and compete with each other.

The result of the competition depends on the flow rate and on the inflow perturbation. When the flow rate is large and the inflow perturbation is small, the Hopf solution suppresses the FDS. But if the inflow perturbation becomes large, the rigid transition to FDS takes place. In this case, the FDS solution expands in space producing the imposed convective Hopf instability. When the flow rate is small, the FDS appears at the sufficiently large inflow perturbation but does not expand in space. The FDS-Hopf domain boundary stays in a fixed position and two solutions coexist.

To describe the competition between the FDS and Hopf solutions, we derived a kind of coupled amplitude equations. Analysis of these equations clarifies the details of the rigid transition to FDS. In particular, we obtained that the critical inflow perturbation for the rigid transition to FDS slightly depends on the initial conditions in the system. This can obstruct the direct numerical or experimental determination of the critical inflow perturbation for the rigid transition to FDS.

In experiments, decreasing of the flow rate may be accompanied with the decreasing of the inflow perturbation. In the domain of the rigid transition to FDS this may result in destruction of the FDS solution even when the flow rate is above the critical value.

Acknowledgement

This work was supported by RFBR grant 03-02-16192.

Appendix A

The Brusselator is rather an artificial model for the reaction–diffusion system. In this appendix, we provide more examples illustrating our effects in two others, more realistic, systems.

As has done above for the Brusselator model, we perform the series of numerical simulations for one-dimensional systems. The left, inflow, boundary is supposed to be constant, while at the outlet the zero flux boundary conditions are applied.

The first our example is the Lengyel–Epstein model. This is the well-known two variable equation set for the chlorite–iodide–malonic acid–starch reaction (CIMA) reaction [26] (we have added the convective therm to these equations):

$$\frac{\partial u}{\partial t} = a - u - \frac{4uv}{1+u^2} + \frac{\partial^2 u}{\partial x^2} - \phi\frac{\partial u}{\partial x}, \qquad \frac{\partial v}{\partial t} = \delta\left[b\left(u - \frac{uv}{1+u^2}\right) + c\frac{\partial^2 v}{\partial x^2} - \phi\frac{\partial v}{\partial x}\right]. \tag{A.1}$$

Here, u and v are the dynamical variables, a and b are the control parameters, c is the ratio of diffusion constants, ϕ is the flow rate, and δ is the rescaling factor also responsible for the differential transport. The dynamics of this model is studied in [27]. The FDS instability for this system is discussed in [16].

Fig. 14 illustrates the spatio-temporal dynamics of this system with homogeneous inflow boundary conditions. For the selected parameters set, the system is in the Hopf domain, and the Hopf instability is absolute. In Fig. 15(a), the small inflow perturbation is applied. It decays right near the inlet. Whole space is still occupied by the Hopf oscillations. But if the perturbation becomes larger, as in Fig. 15(b), the rigid transition to FDS takes place, and the imposed convective Hopf instability is observed. Decreased flow rate in Fig. 16 is insufficient to produce the imposed convective instability. The localized FDS domain appears near the inlet instead. FDS and Hopf solutions coexist in this figure.

The other example is the reaction–diffusion system with the mixed-order nonlinearity. The model equations are derived in [28]. Detailed investigation of the FDS instability in this system is performed in [16].

$$\frac{\partial a}{\partial t} = \delta\frac{\partial^2 a}{\partial x^2} - \delta\phi\frac{\partial a}{\partial x} + \mu - pab - (1-p)ab^2, \qquad \frac{\partial b}{\partial t} = \frac{\partial^2 b}{\partial x^2} - \phi\frac{\partial b}{\partial x} + pab + (1-p)ab^2 - b. \tag{A.2}$$

Here, a, b are the dynamical variables, μ is the control parameter, the parameter $p \in [0, 1]$ measures the strength of the quadratic nonlinearity against the cubic one, ϕ is treated as the flow rate, and δ is responsible for the differential transport.

Fig. 17 demonstrates the rigid transition to FDS for the system (A.2). In panel (a), the inflow perturbation is small. This decays very fast and is not even visible in the figure. The spatio-temporal diagram for the case of the homogeneous boundary looks identical and is not presented. In panel (b), the inflow perturbations is a little bit larger. This results in the rigid transition to FDS and in the imposed convective instability. In Fig. 18, the flow rate is sufficiently small, and the rigid transition to FDS disappears. The localized FDS domain develops near the inlet instead. The FDS-Hopf domain boundary stays in a fixed position, and two solutions coexist. Notice that the spatio-temporal dynamics of the system (A.2) is more complicated than in our previous illustrations: the frequency of the Hopf oscillations becomes different in presence of the constant boundary. The similar effect is discussed in [29,18] for the complex Ginzburg–Landau equation.

We presented two additional examples of the reaction–diffusion systems with flow where the rigid transition to FDS takes place. For these systems, as well as for the Brusselator model, development of the FDS in presence of the absolute Hopf instability depends on the flow rate and on the inflow perturbation. If the flow rate is sufficiently high, increasing of the inflow perturbation results in the rigid transition to FDS and in the imposed convective Hopf instability. But when the flow rate is small, even large inflow perturbation does not produce the imposed convective instability. The localized FDS domain appears near the inlet instead.

References

[1] L.D. Landau, E.M. Lifshitz, Fluid Mechanics, Pergamon, Oxford, 1959.
[2] R.J. Briggs, Electron Stream Interaction with Plasma, MIT Press, Cambidge, MA, 1964.
[3] A. Bers, Space–time evolution of plasma instabilities—absolute and convective, in: M.N. Rosenbluth, R.Z. Sagdeev (Eds.), Basic Plasma Physics of Handbook of Plasma Physics, vol. 1, North-Holland, Amsterdam, 1983 (pp. 451–517).
[4] A.B. Michailovsky, Theory of Plasma Instabilities (Teorija Plazmennykh Neustoichivostei), vol. 1, Atomizdat, Moscow, 1975.

[5] E.M. Lifshitz, L.P. Pitaevskii, Physical Kinetics, Pergamon, London, 1981.
[6] R.J. Deissler, J. Stat. Phys. 40 (1985) 371.
[7] W. van Saarloos, Front propagation into unstable states: marginal stability as a dynamical mechanism for velocity selection, Phys. Rev. A 37 (1988) 211–229.
[8] W. van Saarloos, Front propagation into unstable states. II. Linear versus nonlinear marginal stability and rate of convergence, Phys. Rev. A 39 (1989) 6367–6390.
[9] S.P. Kuznetsov, E. Mosekilde, G. Dewel, P. Borckmans, Absolute and convective instabilities in a one-dimensional Brusselator flow model, J. Chem. Phys. 106 (1997) 7609–7616.
[10] A.B. Rovinsky, M. Menzinger, Self-organization induced by the differential-flow of activator and inhibitor, Phys. Rev. Lett. 70 (1993) 778–781.
[11] P. Andresén, M. Bache, E. Mosekilde, G. Dewel, P. Borckmans, Stationary space periodic structures with equal diffusion coefficients, Phys. Rev. E 60 (1999) 297–301.
[12] M. Kærn, M. Menzinger, Flow-distributed oscillations: stationary chemical waves in a reacting flow, Phys. Rev. E 60 (1999) R3471–R3474.
[13] P. Andresén, E. Mosekilde, G. Dewel, P. Borckmans, Comments on "Flow-distributed oscillations: stationary chemical waves in a reacting flow", Phys. Rev. E 62 (2000) 2992.
[14] M. Kærn, M. Menzinger, Reply to "Comments on 'Flow-distributed oscillations: stationary chemical waves in a reacting flow"', Phys. Rev. E 62 (2000) 2994.
[15] R.A. Satnoianu, M. Menzinger, Non-Turing stationary patterns in flow-distributed oscillators with general diffusion and flow rates, Phys. Rev. E 62 (2000) 113–119.
[16] R.A. Satnoianu, P.K. Maini, M. Menzinger, Parameter space analysis, pattern sensitivity and model comparison for Turing and stationary flow-distributed waves (FDS), Physica D 160 (2001) 79–102.
[17] P.V. Kuptsov, S.P. Kuznetsov, E. Mosekilde, Particle in the Brusselator model with flow, Physica D 163 (2002) 80–88.
[18] P.V. Kuptsov, S.P. Kuznetsov, C. Knudsen, E. Mosekilde, Absolute and convective instabilities in the one-dimensional Brusselator model with flow, Recent Research Developments in Chemical Physics, vol. 4, Transworld Research Network, 2003, pp. 633–658.
[19] M. Kærn, M. Menzinger, A. Hunding, Segmentation and somitogenesis derived from phase dynamics in growing oscillatory media, J. Theor. Biol. 207 (2000) 473–493.
[20] M. Kærn, M. Menzinger, R.A. Satnoianu, A. Hunding, Chemical waves in open flows of active media: their relevance to axial segmentation in biology, J. R. Chem. Soc., Faraday Discuss. 120 (2002) 295–312.
[21] M. Kærn, M. Menzinger, Experiments on flow-distributed oscillations in the Belousov–Zhabotinsky reaction, J. Phys. Chem. A 106 19 (2002) 4897–4903.
[22] J.R. Bamforth, R. Toth, V. Gaspar, S.K. Scott, Scaling and dynamics of "flow distributed oscillation patterns" in the Belousov–Zhabotinsky reaction, PCCP 4 8 (2002) 1299–1306.
[23] A.F. Taylor, J.R. Bamforth, P. Bardsley, Complex pattern development in a plug–flow reactor, PCCP 4 22 (2002) 5640–5643.
[24] I. Prigogine, R. Lefever, J. Chem. Phys. 48 (1968) 1965.
[25] G. Nicolis, I. Prigogine, Self-Organization in Nonequilibrium Systems, Wiley, New York, 1977.
[26] I. Lengyel, I. Epstein, Modelling of Turing structures in the chlorite–iodide–malonic acid–starch reaction system, Science 251 (1991) 650–652.
[27] O. Jensen, V.O. Pannbacker, E. Mosekilde, G. Dewel, P. Borckmans, Localized structures and front propagation in the Lengyel–Epstein model, Phys. Rev. E 50 2 (1994) 736–749.
[28] J.H. Merkin, R.A. Satnoianu, S.K. Scott, The development of spatial structure in an ionic chemical system induced by applied electric fields, Dyn. Stabil. Syst. 15 (2000) 209–230.
[29] A. Couairon, J.M. Chomaz, Primary and secondary nonlinear global instability, Physica D 132 (1999) 428.